

## Periodization of Holocene Climatic Cycles Based on Synchronous Variations in the Magnetic and Geochemical Parameters of the Sediments of Lake Bolshoe Yarovoe (Southwestern Siberia)

L.R. Kosareva<sup>a</sup>, V.P. Shcherbakov<sup>a,b,✉</sup>, D.K. Nurgaliev<sup>a</sup>, N.G. Nurgalieva<sup>a</sup>, N.K. Sycheva<sup>b</sup>,  
V.V. Antonenko<sup>a</sup>, D.M. Kuzina<sup>a</sup>, V.G. Evtyugin<sup>c</sup>

<sup>a</sup> Kazan (Volga Region) Federal University, Institute of Geology and Petroleum Technologies, ul. Kremlevskaya 4/5, Kazan, 420111, Russia

<sup>b</sup> Borok Geophysical Observatory, Schmidt Institute of Physics of the Earth, Russian Academy of Sciences,  
Borok 142, Yaroslavl Region, 152742, Russia

<sup>c</sup> Kazan (Volga Region) Federal University, Interdisciplinary Center for Analytical Microscopy,  
ul. Parizhskoi Kommuny 9, Kazan, 420111, Russia

Received 22 February 2019; received in revised form 22 May 2019; accepted 28 August 2019

**Abstract**—Variations in the magnetic and geochemical properties of the sediments of Lake Bolshoe Yarovoe (Altai Territory) were studied. The data were derived from five core columns (up to 4.5 m long) covering a time interval of more than 8000 years. In addition, coercive spectra were obtained for 792 samples taken every 2 cm. Coercive spectra were then used to identify soft magnetic (10–15 mT) and hard magnetic (35–50 mT) components. The soft magnetic component is detrital, and the hard magnetic component is biogenic, which is confirmed by microscopic studies. Moreover, the samples contain micrometeorite particles. Variations in geochemical properties allow reconstruction of the environmental history of the lake. Sediments in the lower part of the section vary both in the content of ferrimagnetic components and in geochemical properties, which indicates a sharp environmental change between ~6100 and ~7600 years ago. Quasi-periodic alternation of warm (dry) and cool (humid) periods is observed higher in the section, between ~4100 and ~6100 years ago. The variations in the magnetic components are consistent with the environmental changes and can be used for the historical reconstruction.

**Keywords:** lacustrine sediments, Holocene climate, magnetic properties, ferrimagnetic components, magnetotactic bacteria, coercive spectra

### INTRODUCTION

The information value of modern lake sediments is determined by accumulation of minerals, such as iron-bearing ones, that can be used in paleomagnetic, mineralogical, and paleoclimatic studies. In contrast to ocean sediments, lake sequences accumulate at a relatively high speed, which results in a significantly higher resolution (Evans and Heller, 2003). The main factor regulating lake sedimentation processes is the climate. It determines the hydrological and hydrochemical regime of the lake as well as the nature and type of sediments. A large variety of lake types and numerous factors determining the sedimentation process ensure that each lake sequence has its own unique magnetic composition.

Today, the topical issue is the study of sudden and sharp climate changes that occurred in relatively short time intervals (100–1000 years), on both the regional and global scale.

It is generally accepted that small modern salt lakes (that form only in arid and semiarid conditions) are best suited for such studies. Small lakes, in contrast to large water bodies, are more sensitive to climate and environmental changes; therefore, they may contain more detailed “records” of these changes (Zhilich et al., 2017; Krivonogov et al., 2018; Solotchina et al., 2018). Lake Bolshoe Yarovoe is one of the small hypersaline lakes located in the southwest of Siberia. The bottom sediments of this lake are one of the few sources of the data on the composition and genesis of Holocene sediments available in the region. Earlier, pollen and diatom studies were conducted using 23 samples taken from core column no. 3 (Rudaya et al., 2012). Palynological data suggested that there were five zones, so that the quantitative analysis of the data and reconstruction of the biome were carried out (Prentice et al., 1996). This method uses modern ecology, the bioclimatic tolerance range and the geographical distribution of pollen-forming plants to attribute pollen taxa to functional types of plants and to biomes. This method was previously adapted for the reconstruction of North Eurasian biomes (Tarasov et al., 1998). The data provided in

✉ Corresponding author.

E-mail address: shcherb@borok.yar.ru (V.P. Scherbakov)

(Rudaya et al., 2012) are in good agreement with the results of the studies conducted in the framework of this work (see “Discussion”).

Changes in the magnetic properties of sediments very often reflect climate and environmental changes. An increase in the terrigenous magnetic component may be associated with high humidity in the region and increased river inflow; an increase in the bioproductivity of the lake is accompanied by an increase in the number of magnetotactic bacteria (MTB), which can lead to a sharp increase in the authigenic magnetic component due to magnetite or greigite grains produced by these bacteria if their biomass is sufficient. The bioproductivity of lakes is closely related to climate and environmental changes (to the temperature, humidity, and oxidizing conditions, primarily). It is also possible that the changes in the source (the provenance) area or catastrophic events, such as volcanic eruptions, can be the reason for the variations in magnetic parameters.

Coercive spectra (CS) of isothermal remanent magnetization (IRM) contain most of the information about the ferromagnetic component (composition, structure, and content). This topic is developed also in (Kochegura, 1965; Belokon' et al., 1973; Sholpo, 1977; Egl, 2003, 2004a,b; Heslop and Dillon, 2007; Kosareva et al., 2015; Fabian et al., 2016). Such interest in the ferromagnetic component is related to the problem of assessing the contribution of the biogenic component to the remanent magnetization, because the content of biogenic magnetic particles is highly dependent on the paleoclimatic conditions.

As for the magnetic susceptibility of sediments, the paramagnetic component has the greatest influence on it. This is

due to the very low content of ferromagnetic particles in the sediments of most modern lakes, while most of the biogenic materials and water are diamagnetic. The biogenic contribution to the magnetic susceptibility is also determined by the superparamagnetic component formed by the smallest (up to 30 nm) fractions.

The aim of this research is to reveal the nature of the magnetic minerals that can be found in the sediments of Lake Bolshoe Yarovoe (southwest of Siberia, Slavgorod District, Altai Territory) and to analyze changes in their composition and concentrations along the core depth, which are assumed to be the result of (1) changing environmental conditions and deposition rate and (2) formation of chemo-genic and biogenic ferrimagnetic particles. The discussion section features a preliminary reconstruction of changes in environmental conditions in the region over the past 9000 years based on magnetic and geochemical studies.

## CHARACTERISTICS OF THE OBJECT OF RESEARCH AND THE TEST MATERIAL

Lake Bolshoe Yarovoe is a closed salt lake located in the southwest of Siberia, Slavgorod District, Altai Territory (western part of the Kulunda Plain, Fig. 1). It is located at an altitude of about 79 m. The water area is 70 km<sup>2</sup>; the average depth is 4–4.25 m; the maximum depth reaches more than 8 m (this is the deepest lake of the Kulunda Steppe). The lake occupies a deep (up to 25 m) syncline. The total catchment area is approximately 560 km<sup>2</sup>. Salt flats are situated to the east of the lake. The length of the lake is 11.5 km; the

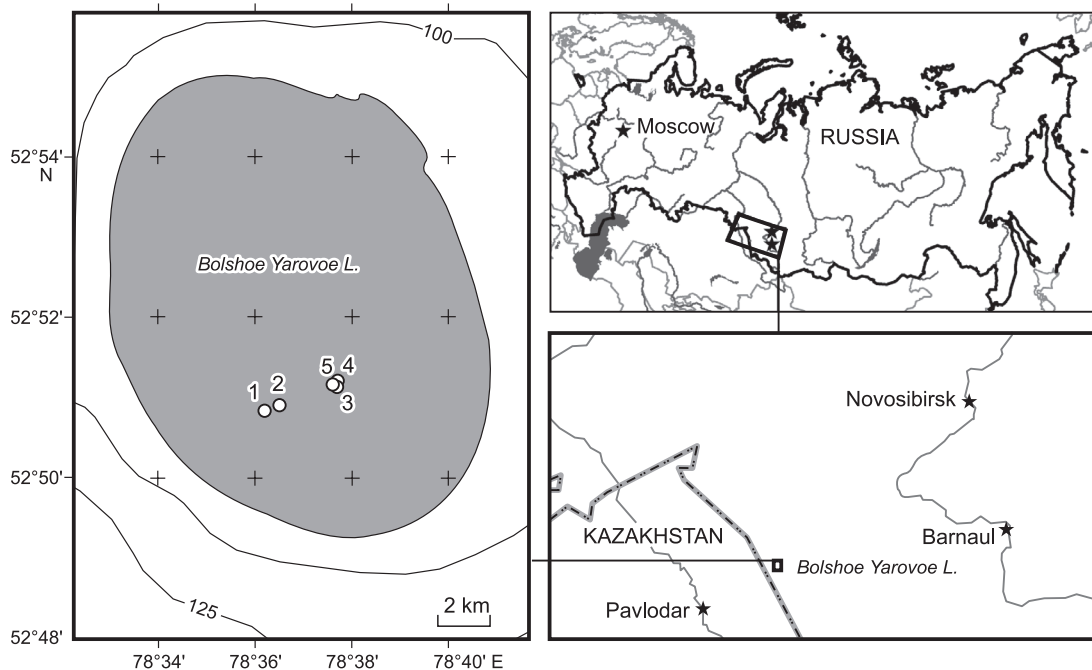


**Fig. 1.** Map of Lake Bolshoe Yarovoe (plotted in ArcGIS 10.3, ESRI, United States). Circles and numbers 1–5 indicate the location of the core sampling.

**Table 1.** Coordinates and main data on core sampling sites

Column	Coordinates		Depth, m	Length of column, m	Number of samples
	N	E			
1	52°50.837′	78°36.195′	7.5	3.3	165
2	52°50.901′	78°36.507′	7.5	3.56	178
3	52°51.156′	78°37.601′	8.0	4.02	201
4	52°51.16′	78°37.606′	8.5	4.26	213
5	52°51.161′	78°37.595′	8.5	4.56	228

maximum width is 8 km (Sidorenko, 1972). The shores are steep and carved with deep ravines. The southwestern shores are very steep and rise up to 20 m. The eastern shores are only 1.5–2 m high. The coastline is smooth and forms a small bay only in the northeastern part. Thanks to such traits of the relief, there is a constant supply of terrigenous material during spring runoff and precipitation events.

In 2008, five core samples were obtained during the expedition of the Institute of Geology and Petroleum Technologies to Lake Bolshoe Yarovoe with the aim of studying the bottom sediments. The sampling points are shown in Fig. 1 and listed in Table 1. In order to find undisturbed stratified sediments, preliminary seismoacoustic studies were carried out (Krylov et al., 2015). The sampling was done using a unique bottom sampler designed and manufactured at Kazan Federal University (Borisov, 2004). This is a 6 m-long piston corer with a vacuum anchor similar to the one used in (Mackereth, 1958). The difference is that it is not gas-dynamic but hydraulic to ensure safety and more careful extraction of sediments (Nurgaliev et al., 1996). The sampler can retrieve core samples that are 70 mm in diameter from the depths of up to 100 m. Layer-by-layer sampling into nonmagnetic cubic plastic containers ( $2.2 \times 2.2 \times 2.2$  cm) for paleomagnetic studies and into marked ziplock bags for laboratory tests was carried out with a step of 2 cm in field, immediately after the core was delivered to the shore.

Lithologically, the sediment is poorly consolidated dark gray silt (top 20–25 cm) alternating with poorly and well consolidated black, gray, and greenish gray sapropel riddled with mudded interlayers.

## RESEARCH METHODS

Four samples of organic material were extracted from core samples nos. 2 and 4 (two from each) to assess the age of the studied sediments.  $^{14}\text{C}$  dating was carried out at the

Swiss Federal Institute of Technology (ETH Zürich). The OxCal v4.2.4 Bronk Ramsey (2013) software and the IntCal 13 calibration curve were used to calibrate the age of the samples. This allowed more accurate determination of the time intervals. The radiocarbon dates are given in the number of years to this day along with the statistical error. The starting point was the year 1950. The radiocarbon dating results (Table 2) suggest that the sediments are of Holocene age.

Magnetic and mineralogical analysis was carried out at the Laboratory of Paleoclimatology, Paleoecology, and Paleomagnetism (Kazan Federal University). The magnetic susceptibility ( $\chi$ ) was measured with MS2 B (Bartington Instruments) at a frequency of 465 Hz with a step of 2 cm using all samples from each core column. A total of 985 samples were studied. The NRM was measured using the JR-4 magnetometer (AGICO). The obtained values were normalized to the volume of the cubic container holding the sample.

Thermomagnetic analysis was carried out at a heating rate of 100 °C/min. For this study, differential thermomagnetic analysis (DTMA) according to induced magnetization was performed using a self-registering torsion magnetometric balance (Burov and Yasonov, 1979; Nourgaliev and Yasonov, 2009). Twenty-six samples taken from core columns nos. 1 and 3 were studied, and thermomagnetic  $J_i(T)$  curves were obtained by heating the samples to a temperature of 800 °C in a field of 0.2 T. In addition, the JRT\_Meter was used to derive the  $J_{rs}(T)$  curve from ten samples taken from core column no. 4. To that end, the samples were initially magnetized in a 1.5 T field and then  $J_{rs}$  was measured as the samples were heated to 700 °C.

Coercive spectrometry studies were carried out for 792 samples taken from columns nos. 1–4. The sampling step was 2 cm. The J\_meter coercive spectrometer (Burov et al., 1986; Iassonov et al., 1998; Enkin et al., 2007; Nurgaliev and Yasonov, 2009) was used for this purpose. The spectrometer allows the automatic measurement of normal remanent magnetization curves of the samples with a volume of 1 cm<sup>3</sup> in the continuously increasing (to 1.5 T) external magnetic field. Curves of normal remanent magnetization and magnetic reversal obtained from a natural magnetic state were used to determine the following petromagnetic parameters: saturation magnetization ( $J_s$ ), saturation field ( $B_s$ ), remanent saturation magnetization ( $J_{rs}$ ), coercive force ( $B_c$ ), and remanent coercive force ( $B_{cr}$ ).

**Table 2.** Results of radiocarbon dating of Lake Bolshoe Yarovoe sediments

Column	Depth, m	Substance	Laboratory number of determination	$^{14}\text{C}$ age	Calibrated age
				years ago	
2	1.55–1.63	Sapropel	ETH-46569	3480±30	3810±80
2	3.13–3.21	Sapropel	ETH-46570	6685±30	7600±60
4	3.81–3.85	Sapropel	ETH-46571	6605±30	7550±70
4	4.15–4.19	Sapropel	ETH-46572	7785±30	8620±60

Microscopic studies of five samples taken from core column no. 4 were carried out in the Interdisciplinary Center for Analytical Microscopy (Kazan Federal University) using the HT7700 Excellence Transmission Electron Microscope (Hitachi). Elemental analysis was performed in STEM mode using the X-Max 80T detector (Oxford Instruments). In addition, studies were conducted using the MERLIN Field Emission Scanning Electron Microscope (Carl Zeiss). The microscope is equipped with the AZtec X-Max energy dispersive spectrometer.

Component analysis of the ferrimagnetic fraction was carried out applying non-negative matrix factorization (NMF) to normal-magnetization spectra (Fabian et al., 2016).

In addition to the magnetic and radiometric studies, geochemical analysis was carried out on samples taken from core columns nos. 1 and 3 every 10 cm, starting 5 cm from the top. A series of geochemical indices and relationships were derived from them. The elemental composition of the lake sediments was determined by X-ray fluorescence analysis. The measurements were carried out using the Bruker S8 TIGER spectrometer. The spectrometer was calibrated with standard samples with SiO<sub>2</sub> matrix. A wide range of

chemical elements was covered by the study – from Na to Ta, W, and Pb. As a result, the contents of 41 chemical elements in the core columns were determined.

## RESULTS

**Core correlation and dating.** Figure 2 shows the variations of  $\chi$  and NRM measured for each of the core samples. The core samples are ordered by distance from the coast. As can be seen, both  $\chi$  and NRM show characteristic sharp peaks, which can be used as a reliable marker for correlation. Gray lines in Fig. 2 reflect the principle of such correlation. However, correlation is a quite complex process. For example, at least layer 5 is missing from core samples 1 and 2, retrieved near the shore. This is most likely due to a sudden fall of the water level and, consequently, a depositional break. In addition, the behavior of  $\chi$  and NRM around the depth of ~250–300 cm in layer 4 of sample 2 is not consistent with what can be seen in other samples. This might be due to the emergence of an ancient pockmark (Krylov et al., 2015). Biogenic methane in the upper part of the sediment raised the

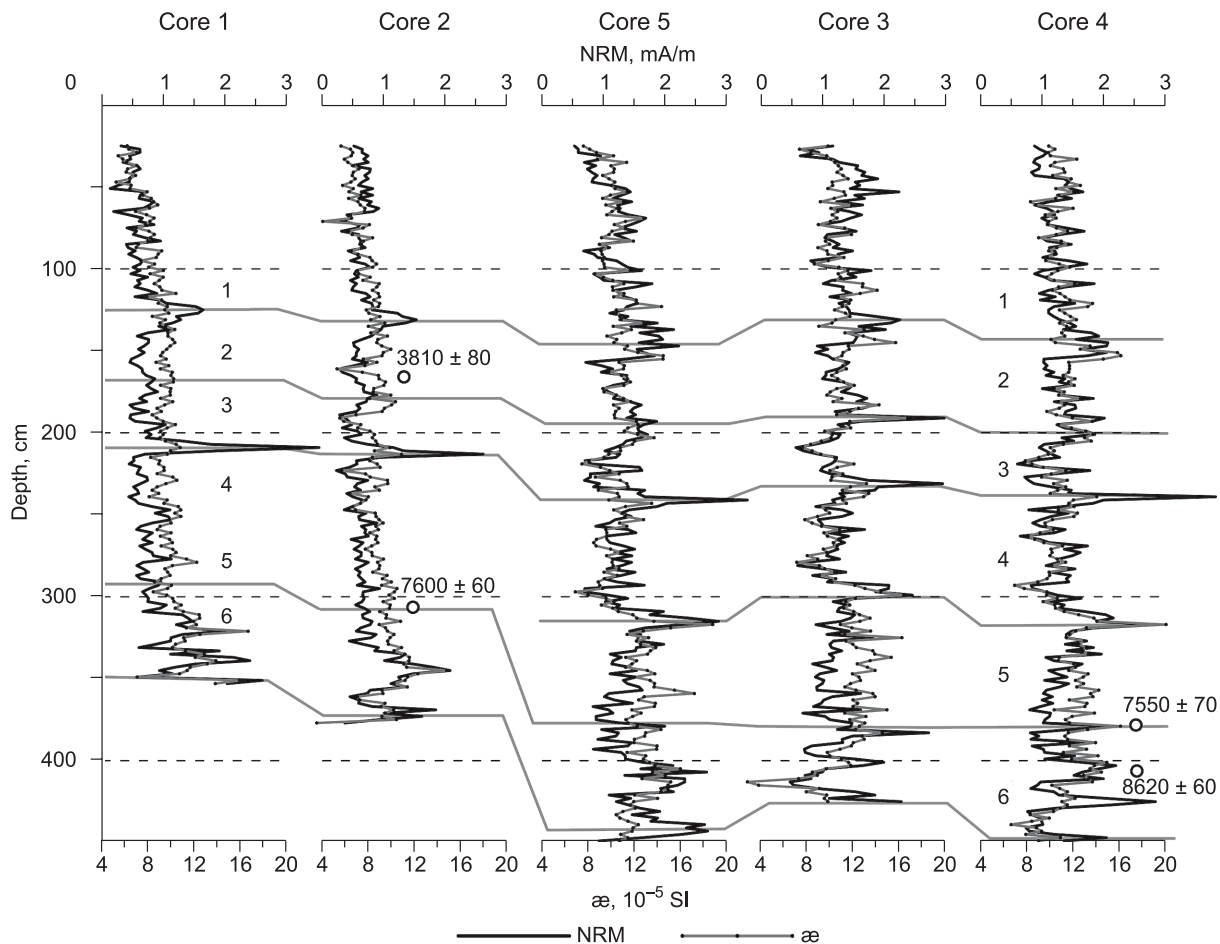


**Fig. 2.** Correlation scheme of the cores of Lake Bolshoe Yarovoe on the basis of their magnetic susceptibility ( $\chi$ ) and magnetization (NRM). Gray lines indicate correlation. Circles show the location of radiocarbon dating and calibrated ages (yr BP). Numbers 1–6 denote interlayers.

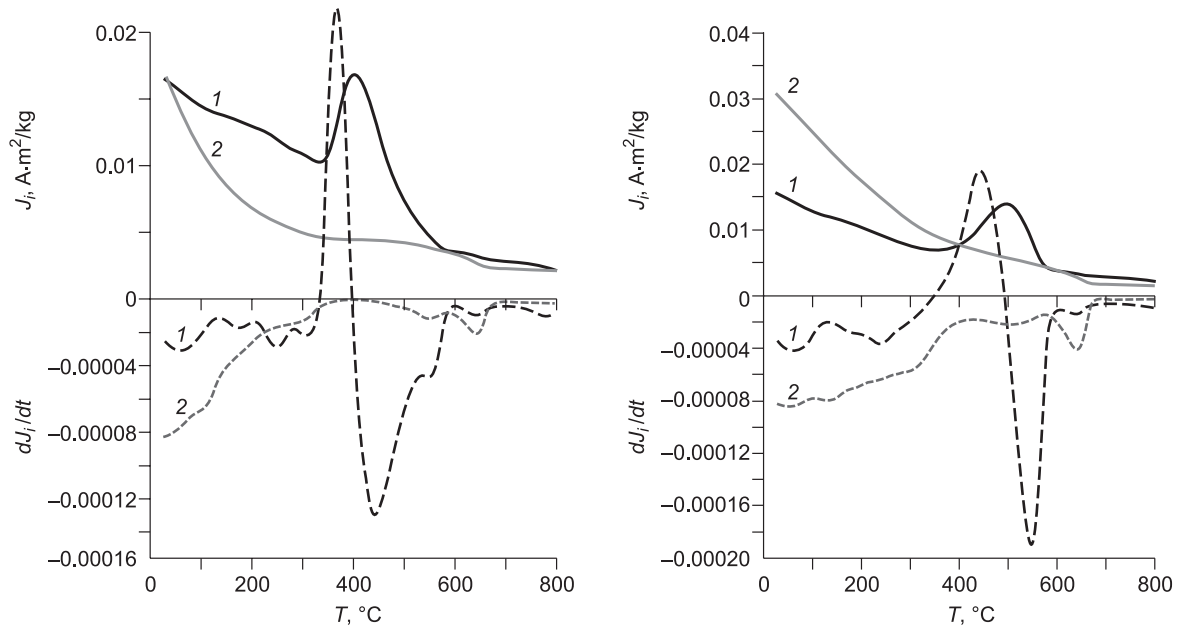


**Fig. 3.** Integral (continuous) and differential (dashed) curves of the first (1) and repeated (2) heating. *a*, sample 407 (group 1); *b*, sample 479 (group 2).

sapropel and filled the pockmark with younger deposits; as a result, the stratigraphic record in this area is lost and replaced by sediments of the same age as the pockmark.

The correlation technique described above and the radiocarbon dating were used together to create an age model of the lake sediment. The dates obtained for sample 2 ( $3810 \pm 80$  yr BP) were carried over to sample 4. Further, all dates were cross-correlated over all core samples.

Thermomagnetic analysis of fresh samples, however, did not provide the data on mineral composition and major magnetization carriers due to extreme heat sensitivity of the sediment (Fig. 3). An endothermic effect associated with the removal of free (and, sometimes, bound) water was observed in all samples at a temperature of 90–180 °C. Two groups of samples can be distinguished based on the thermal curves.

**Group 1** includes the part of the core covering a depth of 33–59 cm. It is characteristic of the group that the magnetization increases starting at 330 °C and then sharply declines at >400 °C (Fig. 3*a*). Most likely, this effect is caused by organic matter and small sulfide particles present in the samples. Sulfides dissociate at temperatures above 330 °C forming magnetite and, therefore, causing an increase in magnetization. The decrease in magnetization at 650 °C, which is particularly evident during the second heating, is caused by hematite that is produced from the oxidation of very small magnetite grains.

**Group 2** includes the part of the core covering a depth of 67–423 cm. The  $J_i(T)$  of the first heating shows an increase in magnetization at 250–500 °C (Fig. 3*b*). In this case, magnetic minerals form from organic matter and various iron compounds (siderite, ferrum oxide, magnetite, sulfides, etc.), which turn into magnetite when heated above 250 °C.

The differential curves of the second heating show the same drop at 650 °C associated with hematite.

The fundamental difference between these groups is the predominance of iron sulfides in the first group.

**The magnetic hysteresis curve** is a very useful tool for studying magnetic grains in rocks and sediments, since the shape of the hysteresis loop and the values of the hysteresis characteristics and their ratios depend on the size of the magnetic grains, which, in turn, carry information on physical and chemical conditions of sedimentation and their changes. The Day–Dunlop plot in Fig. 4 shows the obtained magnetic hysteresis parameters for four core samples. As can be seen from the plot, the samples are characterized by a mixture of single-domain (SD), superparamagnetic (SPM), and multidomain (MD) grains. Indeed, the points in the plot form a long compact arc in the area between the SD + MD grains, on the one hand, and SD + SPM particles, on the other, in which the representative points of all the columns are localized; this indicates the uniformity of the ferrimagnetic fraction, and, therefore, the same reasons that caused changes in the magnetic properties which can be observed in all samples. Note that the arc is parallel to the SD + MD curve and shifted toward the SD + SPM curve. This leads to the suggestion that the ferrimagnetic particles in the samples are represented by a mixture of SD, MD, and SPM grains, the presence of which is also confirmed by electron microscopic analysis.

For **electron microscopic studies**, a number of samples were taken from core 4. As can be seen from Fig. 5, the detrital component in the samples is represented by large allothigenic grains, among which are large grains of magnetite, iron sulfides and sulfates, titanomagnetite, and chrom-

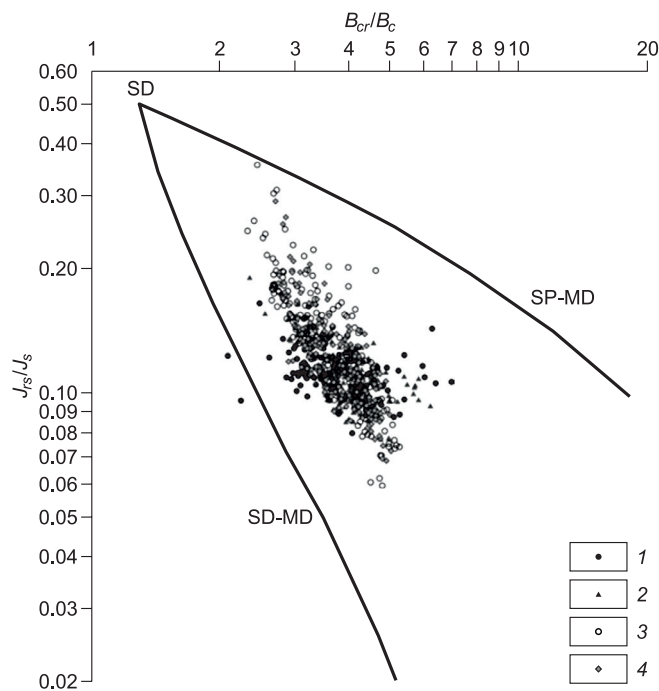


**Fig. 4.** Characteristics of the magnetic structure of grains by hysteresis parameters of Lake Bolshoye Yarvoe sediments on the Day–Dunlop theoretical diagram. SD, Single-domain; MD, multidomain; SP, superparamagnetic grains (Day et al., 1977; Dunlop, 2002). 1–4, Samples from columns 1–4, respectively.

magnetite. This component also includes magnetite spherules ranging in size from 3 to 35 microns. Judging by their shape and surface structure, the spherules are of cosmic origin (Genge et al., 2008). Sample 709 (~1200 years old, taken from a depth of 41 cm) is of particular interest (Fig. 5a), since it contains a large number of such spherules, which may have been introduced into the sedimentation basin by a meteorite which burned up in the atmosphere.

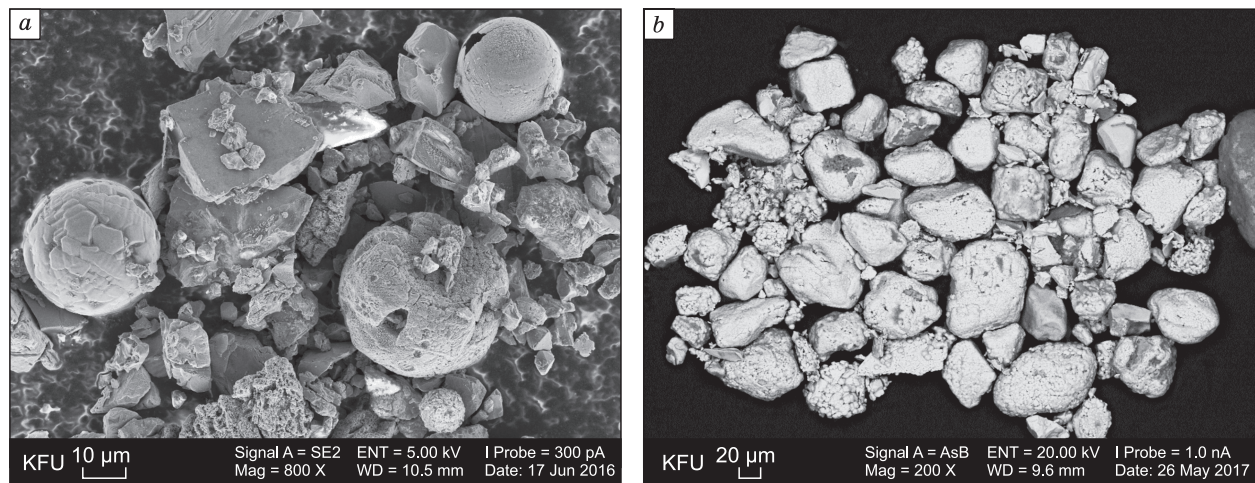


**Fig. 5.** Scanning electron microscopy images of magnetic separate of samples from core 4. a, Sample 709 from a depth of 41 cm, contains magnetite spherules; b, sample 765 from a depth of 153 cm, contains sulfides and sulfates of iron, magnetite, and titanomagnetite.

The biogenic component produced by magnetotactic bacteria is present in all samples and is represented by magnetofossils that vary in shape and size (Fig. 6). For example, in sample 709, magnetofossils have the form of a spindle or an elongated octahedron, 60–200 nm in size (Fig. 6a, c, d). Most particles reach a length of 70–120 nm. In sample 834, a number of elongate octahedral particles ranging in size from 200 to 800 nm (with the majority of particles having a size of 400–500 nm) were found (Fig. 6b). Large (200–300 nm in length) spindle-shaped particles can be found much less frequently. Note that particles of such size (giant magnetofossils) were previously detected in pelagic marine sediments of the South Atlantic (the Kerguelen Plateau), and their occurrence corresponds to the warm period in the history of the Earth (Paleocene–Eocene Thermal Maximum) (Chang et al., 2012).

In addition to SD and MD particles, superparamagnetic particles can also be seen on electron microscopic images (Fig. 7). They form clusters of small grains no larger than 20 nm in size, most likely of bacterial origin.

**Component analysis of normal magnetization spectra by non-negative matrix factorization.** As is well known, cluster analysis implies multidimensional data classification designed to decompose a set of objects into a sum or a product of homogeneous components. Cluster analysis has been the subject of much development in recent decades because of the new opportunities provided by advances in computer technology and, subsequently, the possibility of processing large data sets. One of the analysis methods is non-negative matrix factorization (NMF) (Heslop and Dillan, 2007; Fabian et al., 2016). Briefly, the principle of NMF is as follows: Having an input matrix  $\mathbf{X}$  (usually representing experimental data), the NMF algorithm decomposes it into a product of two lower-ranked matrices  $\mathbf{S}$  and  $\mathbf{A}$  (i.e.,  $\mathbf{X} \approx \mathbf{AS}$ ). Usually,  $\mathbf{S}$  is a matrix of  $J$  components, which are called endmembers, and  $\mathbf{A}$  is a matrix of coefficients reflecting the

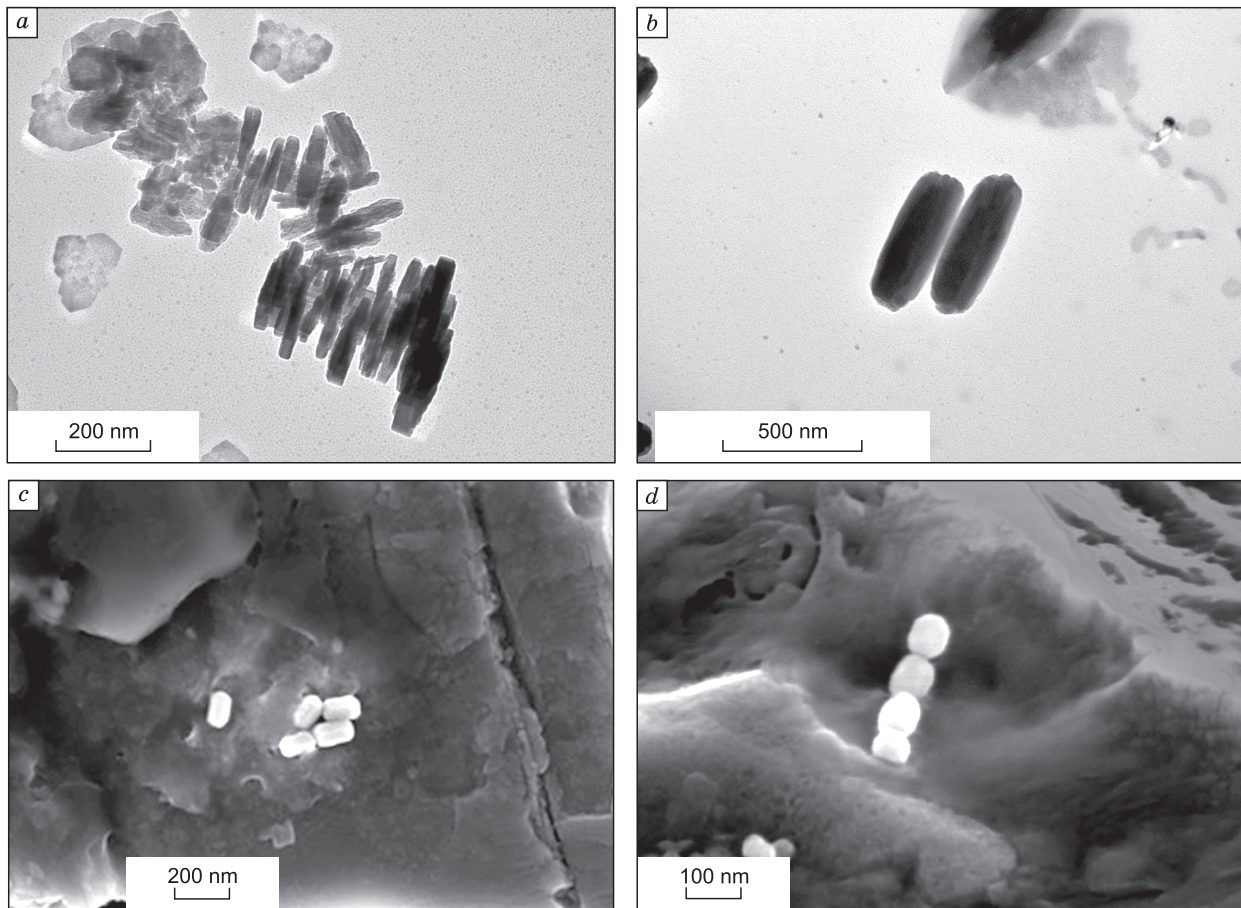


**Fig. 6.** Electron microscopic images of magnetofossils of samples 709 and 834. *a, b*, Transmission microscopy; *c, d*, scanning microscopy; *a, c*, *d*, sample 709, depth 41 cm; *b*, sample 834, depth 291 cm.

contribution of endmembers to the total sum, which should approximate the result of each individual experiment. Basically, the algorithm requires the number of finite elements  $M$  and the initialized matrices  $\mathbf{A}$  and  $\mathbf{S}$ ; in most cases, random numbers distributed uniformly in the interval  $(0, 1)$  are used.

Unlike the principal component analysis, this algorithm implies a strong requirement that all coefficients of the matrix  $\mathbf{A}$  be non-negative. This requirement naturally follows from the physical sense of the problem (the contribution of each endmember cannot be negative). To solve this problem, D. Lee and H. Seung (2001) proposed a multiplicative iteration algorithm, where the Euclidean distance between  $\mathbf{X}$  and  $\mathbf{X}^*$  is calculated as a criterion of accuracy.  $\mathbf{X}$  is the original matrix,  $\mathbf{X}^* = \mathbf{AS}$ :

$$\|\mathbf{X} - \mathbf{X}^*\|^2 = \sum_{ij} (X_{ij} - X_{ij}^*)^2. \quad (1)$$

To minimize it, the following rules for updating matrices  $\mathbf{S}$  and  $\mathbf{A}$  at each step of iteration are used:

$$S_{a\mu} \leftarrow S_{a\mu} \frac{(A^T X)_{a\mu}}{(A^T AS)_{a\mu}}, \quad A_{ia} \leftarrow A_{ia} \frac{(XS^T)_{ia}}{(ASS^T)_{ia}}. \quad (2)$$

It should be noted that the solution obtained by the multiplicative iteration algorithm is not unique; NMF does not guarantee that the only possible decomposition was obtained.

The researchers D. Heslop and M. Dillon (2007) proposed using NMF to decompose a set of  $N$  experimental isothermal remanent magnetization (IRM) curves  $I_{r,n}(B_l)$ , measured in a magnetic field  $B_l$   $\{l = 1, \dots, L\}$ . Accordingly, there are  $N$  coercive spectra  $X_{n,l} = dI_{r,n}/dB$ , so that their complete set can be regarded as a set of vectors  $X_n = \{x_{n,l}\}$  with  $L$  coordinates corresponding to specific values of  $B$ . In this particular case, the coercive spectra were calculated using the IRM curve (Fig. 8, the corresponding section is indicated by a dashed line).

Let us now represent each term as a vector  $\mathbf{S}_j = \{s_{j,1}, \dots, s_{j,L}\}$  with  $L$  components, and approximate  $X_n$  data set by linear expressions

$$X_n^* = A_{n,1}S_1 + \dots + A_{n,J}S_J. \quad (3)$$

$A_{nj}$   $\{n = 1, \dots, N, j = 1, \dots, J\}$  is the non-negative coefficient (weight) matrix. Non-negative coefficients ensure that the linear expression reflects a physical mixture of different physically meaningful elementary coercive spectra (components). Negative  $A_{nj}$  would correspond to a decrease in the

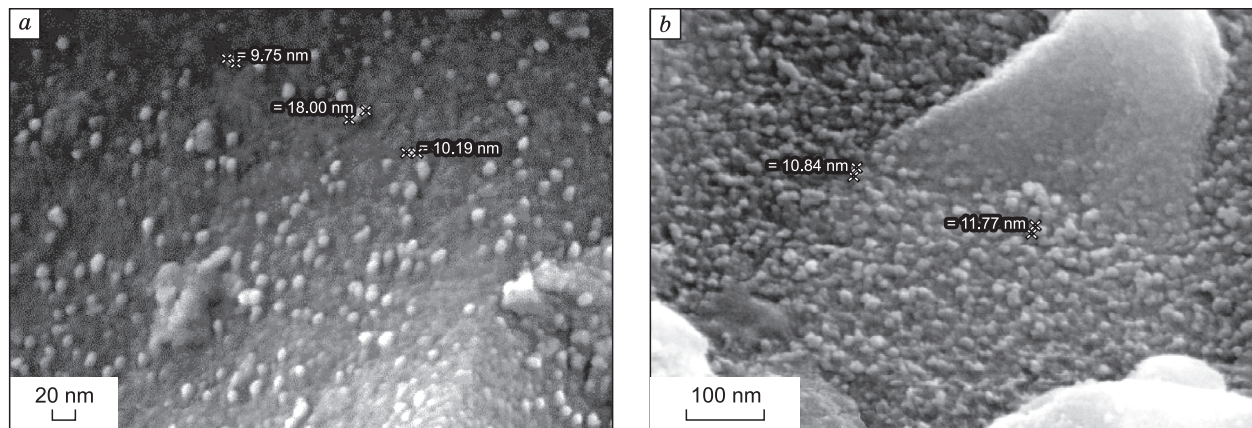


Fig. 7. Scanning electron microscopy images of superparamagnetic particles, sample 709 from the 41 cm depth.

contribution of  $j$  component to IRM, which is not realistic for natural sediments unless they show signs of self-reversal magnetization.

In all four experiments, the magnetic field increased from 0 to 500 mT, with an increment of 0.5 mT and 1 mT for samples 1, 2 and 3, 4, respectively. The obtained coercive spectra were smoothed with a one-dimensional cubic spline and decomposed into two components using the NMF algorithm. To initialize the matrix  $\mathbf{A}$  with dimension  $N \times M$  and the matrix  $\mathbf{S}$  with dimension  $M \times L$ , a pseudorandom number generator was used. The numbers were distributed uniformly in the interval (0, 1).

For ease of interpretation,  $\mathbf{S}_1$  and  $\mathbf{S}_2$  were normalized so that  $M_{rs}(S_j) = \sum_{l=1}^{500} s_{j,l} = 1$ ,  $\{j = 1, 2\}$ . As a result, the coefficients of the matrix  $A_{n,j}$  physically correspond to the contri-

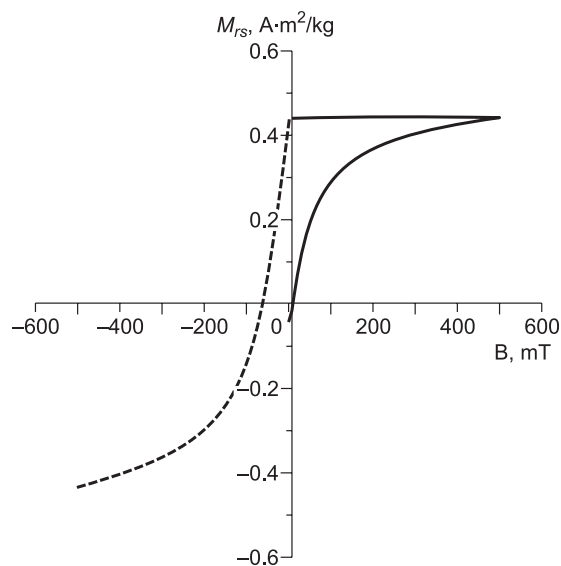


Fig. 8. Sample no. 1 (column 1). The figure illustrates the calculation of the coercive spectrum.

bution of  $\mathbf{S}_j$  component to the remanent magnetic moment  $M_{rs}$  of sample  $n$  (Fig. 9).

Figures 9e, f present the decomposition of coercive spectra obtained from experimental data for two samples taken from core 3 at depths of 143 and 231 cm, respectively. The figures show that the complete signal (upper solid line) is almost fully represented by a sum of just two components (upper dashed line). Attempts to add the third component did not lead to anything new, since it either coincided with one of the previous components or reduced to zero. The maximum of the soft component  $S_2$  (dotted line) is in the range of 10–15 mT, while the maximum of the hard component  $S_1$  (solid line) is in the range of 35–50 mT. Earlier, R. Egli (2004b), using data from detailed laboratory studies, distinguished five types of ferrimagnetic components that can be found in modern lake sediments: “EX” (extracellular magnetite); “D” (detrital magnetite); two types of magnetosomes: “BS” (biogenic soft) and “BH” (biogenic hard); and the highly coercive component “H”. In these terms, the hard component  $S_1$  with a peak value of 35–50 mT should be considered the “BS” component, while the soft component  $S_2$  is the “D” component. In addition to these components, which can be seen on the hysteresis loop, the “EX” component is present in the samples. It is represented by SPM grains, as can be seen from the Day plot (Fig. 4) and electron microscopic images (Fig. 7).

Figure 10 shows the dependences of  $M_{rs}(x)$ ,  $A_1(x)$ , and  $A_2(x)$ , where  $x$  is the depth. It is interesting to note that the peaks on  $M_{rs}(x)$  curves might be caused by a sharp increase in both the soft and hard components, either separately or at once. In other words, increases in  $M_{rs}$  within some time intervals might be caused by either increased bioproductivity of MTB or increase in the amount of the detrital component.

All the main peaks correlate very well except for the interval of ~300–375 cm in samples 3 and 4, which is absent in samples 1 and 2 (Fig. 2), probably because of a sudden fall of the water level and, consequently, a depositional break. Figure 10 shows five sections (I–V), which correlate

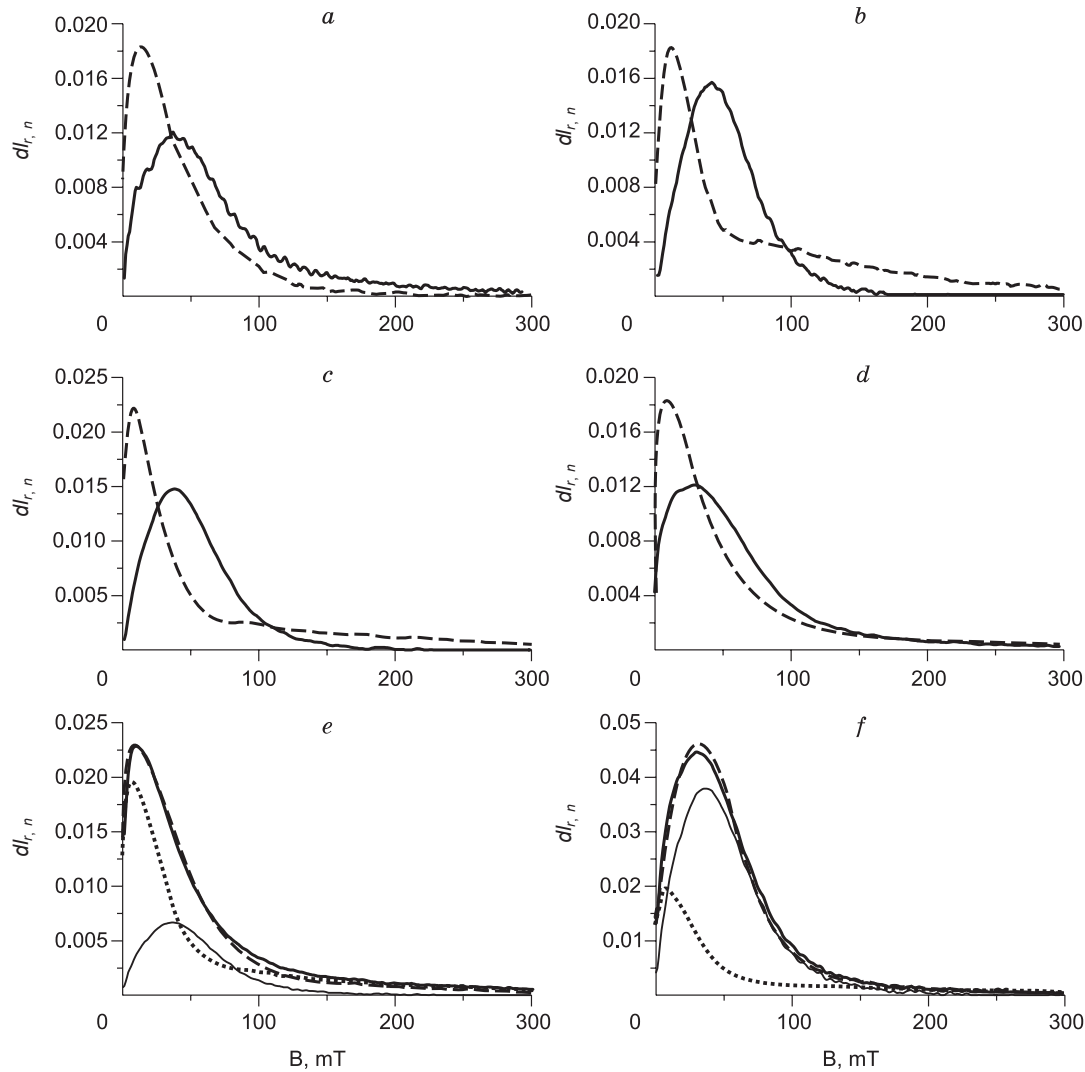


**Fig. 9.** Graphs of the decomposition components  $S_1(B)$  and  $S_2(B)$  for cores 1–4, respectively (a–d); comparison of coercive spectra from experimental data and their approximation by the sum of two components for samples from core 3 (e–f). Thin solid line denotes matrix  $\mathbf{X}$ , whereas dashed line denotes matrix  $\mathbf{X}^*$ . Sample depths 143 (e) and 231 (f) cm. A bold solid line and a dotted line show the graphs of components  $S_1(B)$  and  $S_2(B)$ , respectively.

in details in all samples, showing a similar relationship between  $A_1(x)$  (red line) and  $A_2(x)$  (blue line).

Sections II and V show a good correlation between  $A_1(x)$  and  $A_2(x)$ . The increase in the soft (detrital) component is accompanied by the increase in the hard biogenic component. In other sections, the relationship between the components is more complex, but the correlation between the samples is good. The highest concentration of the soft biogenic component is observed in section III. However, it stands out against the minimum detrital component. The similar pattern can be seen in all samples. In section I, the shift between the peaks of  $A_1$  and  $A_2$  is observed in all samples. First, only the peak of the detrital component can be observed. Then, as it declines, the biogenic component becomes more prominent. Section IV is the most complex; components  $A_1$  and  $A_2$  behave differently in sample 2. As

was mentioned before, this is probably due to the interference of the ancient pockmark. Thus, variations in the magnetic components correlate well in all samples. This justifies the attempt to separate magnetic fractions in lake sediments.

#### Climate variations according to geochemical data.

Among the large number of geochemical markers (Kosareva, 2018), the Ca/Mg ratio and the SrO content are the most informative in this case. A decrease in the Ca/Mg ratio indicates an increase in magnesium and magnesium calcite, which may be due to an increase in water salinity caused by intense evaporation. This is also confirmed by cessation of aragonite sedimentation and onset of halite sedimentation (Kosareva, 2018). Thus, the Ca/Mg ratio represents evaporation processes in the lake (Sun et al., 2010; Zhong et al., 2012; Wang et al., 2013). On the other hand, the increased Sr content in lake sediments can be associated with intense

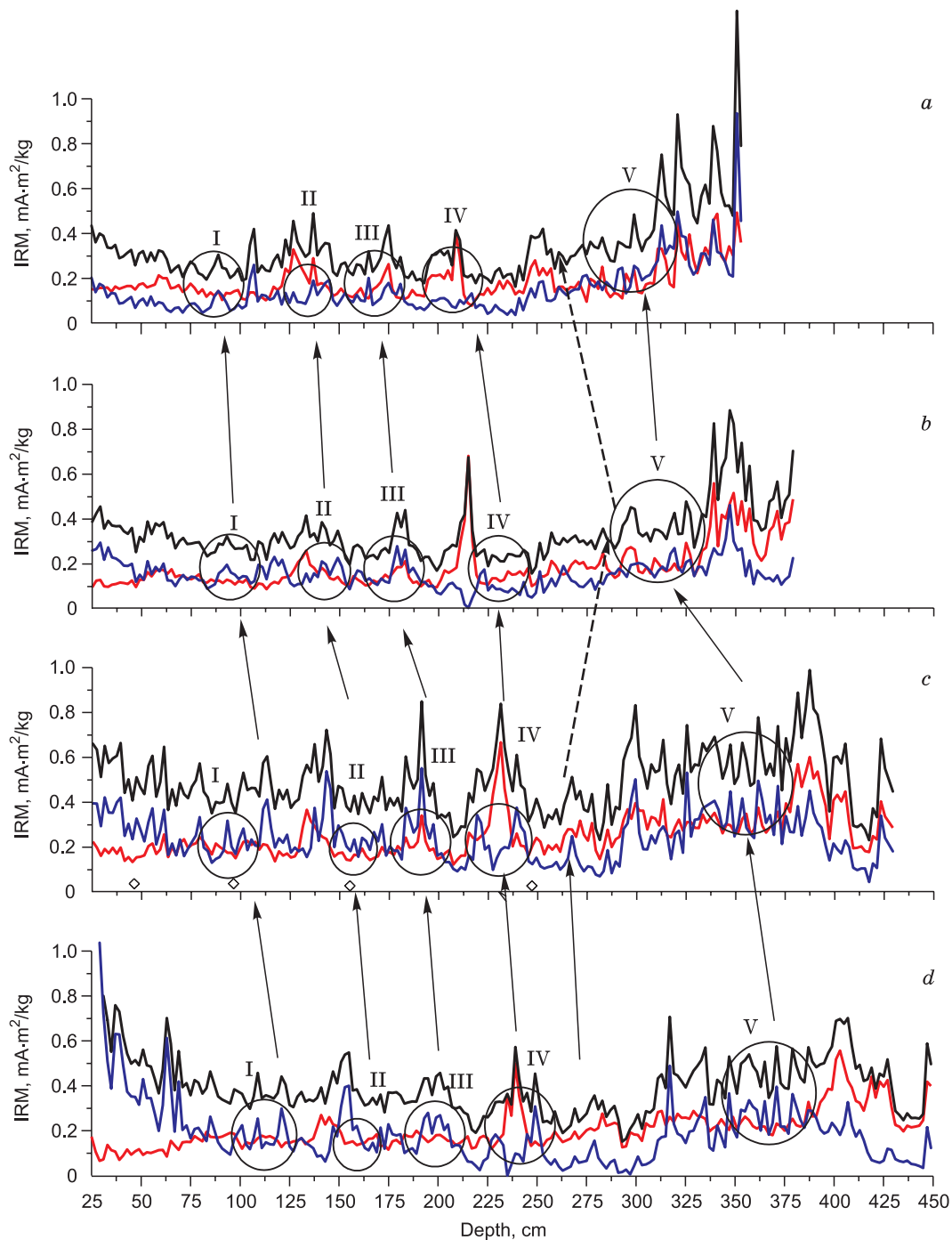


**Fig. 10.** Intensity graphs  $A_1(x)$  (red line) and  $A_2(x)$  (blue line) along the core (bottom). The black line shows the intensity of  $M_{rs}(x)$ . *a–d*, Cores 1–4, respectively. Arrows and circles indicate similar patterns on the graphs.

chemical weathering and the removal of Sr from the rocks of the catchment area (Zhong et al., 2012). That is, this parameter characterizes the general water balance in the area and reflects the water input into the lake. Decreasing SrO content and increasing concentration of Br upsection can also be an indirect indicator of climate aridization in the Holocene, which is clearly observed on the example of the Lake Yarovie sediments (Kosareva, 2018).

Figure 11 shows the correlation between the CaO/MgO ratio and the SrO content for samples 1 and 3. As can be seen, the curves show similar behavior, which is consistent with the detected geochemical variations within the entire lake. There are some discrepancies in the lower part of the section: Layer 5 (300–375 cm; Fig. 2) in sample 3 is not present in sample 1 most likely for the above-mentioned reason (fall of the water level). The variations in geochemi-

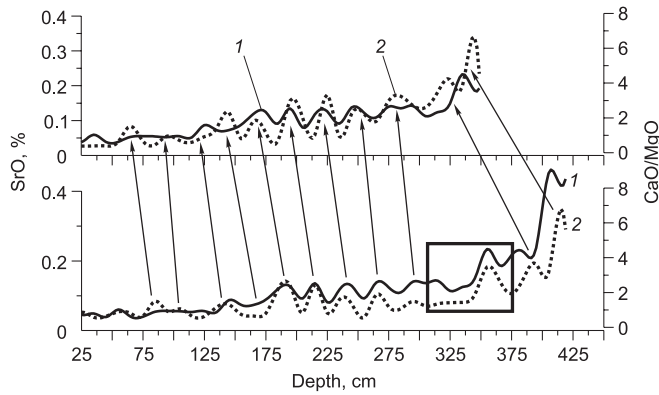


**Fig. 11.** Variations in geochemical ratios in cores 1 (top) and 3 (bottom). 1, CaO/MgO ratio; 2, SrO content. In the square on core 3, there is a section (layer 5 in Fig. 2) that is most likely missing in core 1. The arrows connect the supposed matches of extreme values of SrO content on the graphs for different columns.

cal parameters are relatively easy to explain. A minimum of SrO corresponds to a decrease in the water input and a decrease in the total “humidity” of the catchment area, and a minimum of the CaO/MgO ratio corresponds to increased salinity, i.e., intense evaporation. In other words, the minimum values mean the commencement of a dry and hot period, and, vice versa, the maximum values correspond to a cold and humid climate. In most of the section, consistent

quasi-periodic variations of the indicated parameters are observed. As a rule, warming leads to an increase in salinity.

## DISCUSSION

**The impact of climate change on the magnetic fraction composition.** In order to determine to what extent the magnetic properties of the sediment reflect climate changes, it is first necessary to identify climate trends from independent data (geochemical data in this case). Cold and humid periods, as well as warm periods with an increase in salinity, were distinguished based on the geochemical relations mentioned above (Kosareva, 2018). Sample 3 was selected for the final analysis, which also included detailed geochemical studies. This sample was taken far from the coast (in contrast to sample 1, which was subjected to geochemical analysis, too), so that it should be less prone to the coastal effects and reflect climate changes better. All the variations in geochemical parameters and, consequently, the environment can be confidently traced in both samples.

Figure 12 shows the variations of geochemical parameters alongside the magnetically hard biogenic component  $A_1$  and magnetically soft detrital component  $A_2$ . It should again be emphasized that in most cases there is a good correlation between the geochemical parameters. This indicates that the climate varied from dry to humid in this area. Moreover, these variations are regular, with a period of about 500–

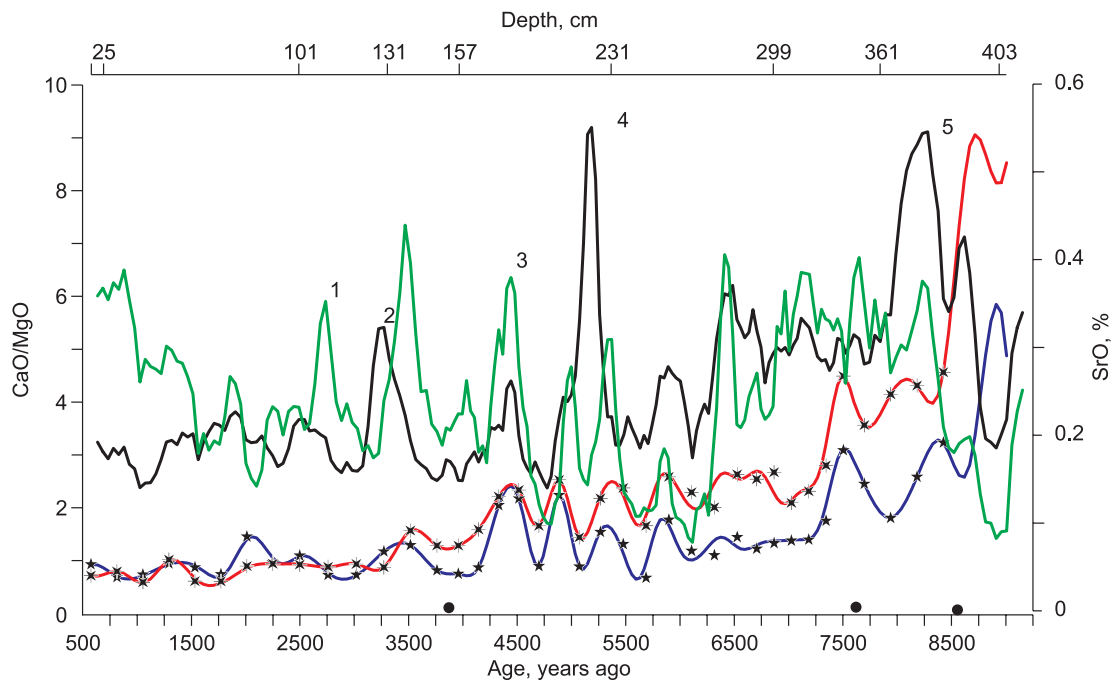


**Fig. 12.** Variations in the geochemical and magnetic parameters of sediments in core 3. The red line is the CaO/MgO ratio (left scale); the blue line is the SrO content (right scale). The stars on these curves are the source data, and the solid lines are the spline interpolation. The black line is the value of the hard biogenic component  $A_1$ , whereas the green line is the value of the soft component  $A_2$  (right scale). The depth scale is shown at the top; the time scale is made on the basis of radiocarbon dating (black circles) and the correlation between the cores (Fig. 2).

600 years. This periodicity is most clearly seen in the interval from 7500 to 3000 years ago. Climate variations of similar duration in the Holocene were discovered earlier by many researchers on the basis of paleoclimate indicators and are usually associated with solar activity (Obrochta et al., 2012). Trends in geochemical parameters clearly demonstrate a general tendency toward a decrease in humidity, which is consistent with Holocene climate variations observed in Siberia (Khotinskii, 1977). This is also confirmed by the presence of gypsum in the section, the decrease in the aragonite content, and increase in the halite content upsection (Kosareva, 2018). The similar trends can be also observed in the hard biogenic component  $A_1$ . This fact is particularly interesting in regard to magnetotactic bacteria, because water salinity may have an impact on MTB population. Indeed, in the lower part of the section (>7500 years ago), the highest values of the hard component  $A_1$  and both geochemical parameters are observed, which is indicative of low salinity and cold climate. In this part of the section, there is no evident correlation between the geochemical parameters (there is an inverse correlation here, in fact).

In the interval from 6500 to 3500 years ago, there is a correlation between the variations of the soft detrital component  $A_2$  and the geochemical parameters, which is quite natural: A great amount of elastic (including magnetic) material is introduced into the basin with water. It should also be noted that the magnetization of the soft detrital component  $A_2$  does not decrease with time. This indicates that there was no catastrophically rapid decrease in water inflow, and salinity increased mainly due to intense evaporation. Moreover, the eastern shore is low, and an increase in the water level by more than 1.5–2.0 m from the current position could have led to a sharp increase in the lake area and, consequently, evaporation. Sedimentation rate should be taken into account when calculating quantitative correlations between the detrital component and the water inflow. Unfortunately, there is a lack of radiocarbon data, especially in the upper part of the section.

As can be seen from the above, both the hard and soft components show rather consistent behavior, at least after 6500 years ago, though the curve for the soft component in sample 1 is not so well expressed. Figures 11 and 12 show that the evolution of both geochemical and magnetic parameters has common features both in general trends and in time scales of hundreds of years. Obviously, such patterns can be explained only by the influence of common external factors, namely, climate and the environment. Since sample 3 shows the best “synchronization” of the parameters, further presentation of the study and its results will be based on the data obtained for this sample and summarized in Fig. 12.

In the lowest part of the section, in the Boreal period ( $t \approx 8800$  years), geochemical parameters increase sharply, which is indicative of low salinity and low temperature. At the same time,  $A_1$  and  $A_2$  values are abnormally small, which means the almost complete absence of detrital inflow and the low bioproductivity of MTB. This may indicate ice con-

ditions at the time. Data on glacial activity in Norway (Erdalen Event, which happened  $\sim 9400$  years ago) (Dahl et al., 2002) and cold climate conditions in China (Zhou et al., 2007) support this hypothesis. Then, over the course of just a few hundred years, the geochemical parameters rapidly decline indicating the transition from a very cold to a relatively warm Boreal period, accompanied by melting snow and increased water inflow. This entails a sharp increase in the oxygen saturation and detrital inflow, which contributes to the MTB population and, consequently, the dramatic increase in the magnetic signal (though a slight decrease can be observed in  $A_1$  and  $A_2$  at  $t \approx 8600$  years). However, as can be seen from Fig. 12, this warm period ends abruptly with slight increase in geochemical parameters at  $t \approx 8500$ – $8000$  years followed by a sharp peak ( $\sim 8200$  years ago) of both ferrimagnetic components (the hard component shows the most impressive growth). Such behavior of the geochemical parameters and the magnetic signal may mark the commencement of the next cold and humid period, which can be associated with the global cooling separating the Atlantic and Boreal stages.

About 7200 years ago, the climate became drier and warmer, which is reflected by the decline in geochemical parameters. Moreover, the values of the parameters stabilized and began to vary in phase, which was not a characteristic of the previous period. Such a change in the behavior of the geochemical parameters indicates climate changes. However, even if cold and humid periods alternated with warm and dry periods every 500–700 years at  $t < 7200$  years, in earlier eras there is no such clear periodicity, and humid periods could be also warm ones. The same is true for the values of  $A_1$  and  $A_2$ . Their maxima at  $t < 7200$  years coincide with, or are close to, the maxima of CaO/MgO and SrO (with few exceptions), but there is no such correlation downsection. All this taken together suggests that such a synchronous quasi-periodic regime marks a transition between the Boreal and the Atlantic period that started in this area later than in Europe, i.e.,  $\sim 7200$  years ago. It should also be noted that the maximum contribution of the hard biogenic component to  $M_{rs}$  is confined to the humid (low salinity and transgression) periods. On the other hand, humid conditions come alongside a great amount of detrital material including magnetically soft minerals. Thus, the maximum of  $A_2$  should coincide with the maximum of SrO, CaO/MgO, and  $A_1$ , as can be observed in Fig. 12.

The hard biogenic component has a wide and pronounced peak around 5100–5250 years, which needs to be discussed separately, because the soft detrital component shows two maxima separated by a deep minimum at the time. This means that the peak falls out of the common pattern: It stands out against the minima of all the other curves (including the minimum of  $A_2$ ), which is indicative of warm and dry periods. The magnitude of this peak brings up the discovery of giant magnetofossils in the bottom sediments of the lake. According to (Chang et al., 2012), giant magnetosomes are formed under hyperthermal conditions. Based on

this, it can be assumed that this period was characterized by high temperatures and overall dryness, that is, it falls into the Holocene Climatic Optimum (5000–6000 years ago). The conditions for the development of giant magnetofossils were favorable at the time, and this led to a sharp increase in the hard biogenic component. Unfortunately, there is no direct evidence of such magnetosomes in sample 3. However, electron microscopy data obtained for core sample 4 confirm that the vast majority of the biogenic magnetic particles found in sample 834, taken from a depth of 291 cm, have a size of 400–500 nm. This sample

is ~5750 years old and also belongs to the Holocene Climatic Optimum, when the average temperature was higher than today, so the giant magnetofossils could have been formed at that time.

As for the upper part of the core, it should be noted that for the sediments younger than 2500 years (the beginning of the Subboreal), the relationship between the CaO/MgO ratio, the SrO content, and the magnetic characteristics becomes unshaped (Fig. 12). Apparently, this is due to the invariable CaO/MgO ratio (against a background of the climate aridization and the increase in salinity to maximum values).

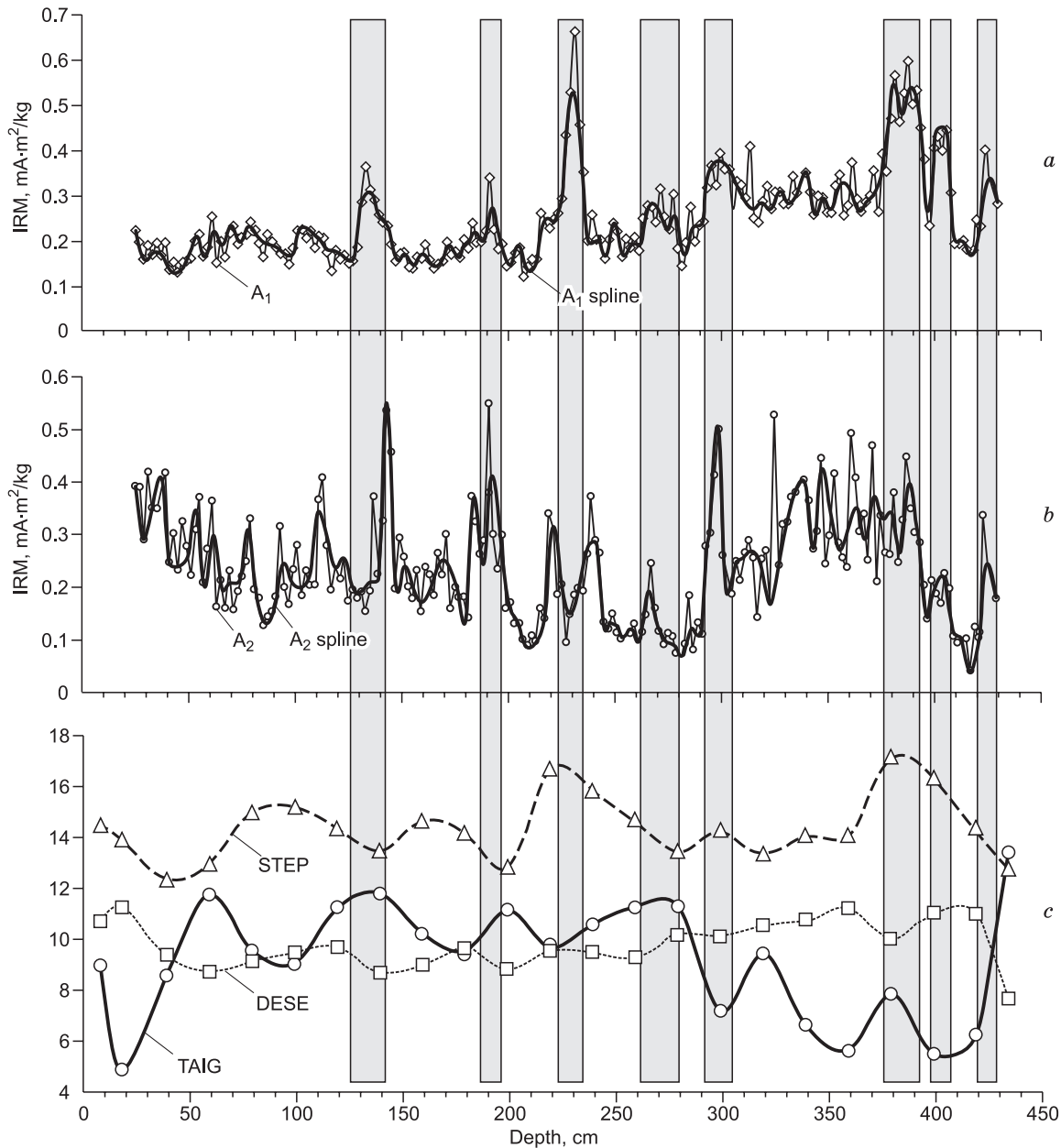


**Fig. 13.** Variations in the magnetic and pollen parameters of sediments in core 3. *a*, Variations in the magnetization of the hard biogenic component  $A_1$ ; *b*, variations in the magnetization of the soft detrital component  $A_2$ ; *c*, variations in the intensity (c.u.) of taiga (TAIG), desert (DESE), and steppe (STEP) biomes (Rudaya et al., 2012). Gray bands show zones with magnetotactic bacteria in the lake, which coincide with zones of the maximum inverse correlation between taiga and steppe biomes.

The fact that the Atlantic period shows a clear alternation of cold and humid stages with warm and dry ones allows estimation of the climate periodicity. The time interval of 7200–3000 years in Fig. 12 is characterized by the most prominent periodicity in the curves. Simple estimates by the number of minima and maxima in this time interval result in the period of about 500–600 years. Note that the estimate is made on the basis of two independent geochemical parameters and the magnetic signal, which ensures its reliability. As for the duration of the period, it turns out to be significantly shorter than Bond's 1500-year cycle (Bond et al., 1997).

An interesting pattern is revealed when comparing the data on the development of MTB in the lake with the results of the pollen analysis (Rudaya et al., 2012). Figure 13 shows the variations in the steppe, taiga, and desert biomes detected in the samples taken from core 3, as well as the magnetic data, i.e., the variations in the hard biogenic component ( $A_1$ ) and the soft detrital component ( $A_2$ ). First, there is a good inverse correlation between the steppe and taiga biomes (Rudaya et al., 2012). This is an interesting fact, which indicates that most of the changes were caused by the confrontation between the taiga and steppe conditions. This process is periodical, too. There were seven cycles of various durations (~600, 1200, and 1800 years) over ~9000 years. It is possible that these are combinations of the cycles that we have identified above. They may not completely coincide with geochemical and magnetic data due to phase delay and multifactorial dependence of the biota on environmental conditions. However, this matter requires further research and more accurate dating.

It is also worth noting that all the peaks of the biogenic component  $A_1$  fall in the areas of maximum inverse correlation between the taiga and steppe biomes. This undoubtedly points to the connection between the development of magnetotactic bacteria in the lake and climatic changes, which are clearly reflected in the paleobotanical data. In four of the eight cases of such a correlation (gray lines in Fig. 13), the intense development of MTB coincides with the maximum of the steppe biome and the minimum of the taiga biome; in four other cases the dependence is just the opposite. At least two possible explanations of this can be found. The first one implies the most "steppe" conditions, when the arid climate caused a sharp increase in the total bioproductivity leading to the occurrence of significant anomalies (for example, at depths of 230 and 385 cm, see Fig. 13). Another option is related to the detrital inflow (including magnetic minerals) contributing to the development of MTB in the lake. This also leads to a decrease in salinity, which also contributes to the development of MTB. Such conditions may occur if taiga outcompetes steppe.

## CONCLUSIONS

1. Coercive spectra of four core samples of the Holocene age taken from Lake Bolshoe Yarovoe were obtained and analyzed. The spectra were then used to identify soft (detr-

tal) (10–15 mT) and hard (biogenic) magnetic (35–50 mT) components;

2. The climate history of the lake was reconstructed based on the variations in the magnetic and geochemical properties. In the studied region, the climate changed from Boreal to Atlantic about 7200 years ago, i.e., this happened much later than in Europe. The Atlantic period was replaced by the Subboreal about 2500 years ago;

3. The Atlantic period shows clear symbiotic changes in the weathering indices ( $\text{SrO}_2$  and  $\text{CaO/MgO}$ ), which corresponds to the alternation of warm (dry) and cold (humid) stages with a period of ~500 years. The same period is also well traced in variations of the biogenic and detrital magnetic components;

4. The changes in the biogenic (hard) component are associated with the productivity of magnetotactic bacteria and correlate well with both the cold and humid and hot and dry periods;

5. It has been established that the peaks of the biogenic component  $A_1$  fall into the areas of maximum inverse correlation between the taiga and steppe biomes, distinguished by pollen analysis. They reflect the relationship between the magnetic signal and climate changes detected by paleobotanical studies (Rudaya et al., 2012).

The work was performed according to the Russian Government Program of Competitive Growth of Kazan Federal University. The work of Kuzina D.M. was funded by the subsidy allocated to Kazan Federal University for the state assignment 671-2020-0049 in the sphere of scientific activities.

Shcherbakov V.P. expresses gratitude to the Russian Science Foundation for the financial support (grant no. 18-17-00251) of the analysis of geochemical and magnetic data. The calculations by the non-negative matrix factorization algorithm were supported by state assignment of IPE RAS.

## REFERENCES

- Belokon', V.I., Kochegura, V.V., Sholpo, L.E., 1973. Methodology of Paleomagnetic Studies of Rocks [in Russian]. Nedra, Leningrad.
- Bond, G., Showers, W., Cheseby, M., Lotti, R., Almasi, P., deMenocal, P., Priore, P., Cullen, H., Hajdas, I., Bonani, G., 1997. A pervasive millennial-scale cycle in North Atlantic Holocene and glacial climates. *Science* 278 (5341), 1257–1266.
- Borisov, A.S., 2004. The Technological Support of Paleomagnetic Studies of Modern Lake Sediments. Dr. Sci. Thesis [in Russian]. Kazansk. Gos. Univer., Kazan.
- Burov, B.V., Yasonov, P.G., 1979. Introduction to Differential Thermomagnetic Analysis of Rocks [in Russian]. Izd. Kazansk. Gos. Univ., Kazan.
- Burov, B.V., Nourgaliev, D.K., Yasonov, P.G., 1986. Paleomagnetic Analysis [in Russian]. Izd. Kazansk. Gos. Univ., Kazan.
- Chang, L., Roberts, A.P., Williams, W., Fitz Gerald, J.D., Larrasoana, J.C., Jovane, L., Muxworthy, A.R., 2012. Giant magnetofossils and hyperthermal events. *Earth Planet. Sci. Lett.* 351–352, 258–269.
- Dahl, S.O., Nesje, A., Lie, Ø., Fjorðheim, K., Matthews, J.A., 2002. Timing, equilibrium-line altitudes and climatic implications of two early-Holocene glacier readvances during the Erdalen Event at Jostedalbreen, western Norway. *The Holocene* 12 (1), 17–25.

- Day, R., Fuller, M., Schmidt, V.A., 1977. Hysteresis properties of titanomagnetites: Grain-size and compositional dependence. *Phys. Earth Planet. Inter.* 13 (4), 260–267.
- Dunlop, D.J., 2002. Theory and application of the Day plot ( $M_{rs}/M_s$  versus  $H_{cr}/H_c$ ). *J. Geophys. Res. Solid Earth* 107 (B3), 2046–2067.
- Egli, R., 2003. Analysis of the field dependence of remanent magnetization curves. *J. Geophys. Res. Solid Earth* 108 (B2), 1–25.
- Egli, R., 2004a. Characterization of individual rock magnetic components by analysis of remanence curves. 1. Unmixing natural sediments. *Stud. Geophys. Geod.* 48 (2), 391–446.
- Egli, R., 2004b. Characterization of individual rock magnetic components by analysis of remanence curves. 2. Fundamental properties of coercivity distributions. *Phys. Chem. Earth* 29 (13–14), 851–867.
- Enkin, R.J., Baker, J., Nourgaliev, D., Iassonov, P., Hamilton, T.S., 2007. Magnetic hysteresis parameters and Day plot analysis to characterize diagenetic alteration in gas hydrate-bearing sediments. *J. Geophys. Res. Solid Earth* 112 (B6).
- Evans, M.E., Heller, F., 2003. *Environmental Magnetism: Principles and Applications of Enviromagnetics*. Academic, San Diego.
- Fabian, K., Shcherbakov, V.P., Kosareva, L., Nourgaliev, D., 2016. Physical interpretation of isothermal remanent magnetization end-members: New insights into the environmental history of Lake Hovsgul, Mongolia. *Geochem. Geophys. Geosyst.* 17 (11), 4669–4683.
- Genge, M.J., Engrand, C., Gounelle, M., Taylor, S., 2008. The classification of micrometeorites. *Meteorit. Planet. Sci.* 43 (3), 497–515.
- Heslop, D., Dillon, M., 2007. Unmixing magnetic remanence curves without a priori knowledge. *Geophys. J. Int.* 170 (2), 556–566.
- Iassonov, P.G., Nourgaliev, D.K., Bourov, B.V., Heller, F., 1998. A modernized coercivity spectrometer. *Geol. Carpathica* 49 (3), 224–226.
- Khotinskii, N.A., 1977. *Holocene of Northern Eurasia* [in Russian]. Nauka, Moscow.
- Kochegura, V.V., 1965. On the analysis of the normal remanent magnetization curve, in: *The Present and Past of the Earth's Magnetic Field* [in Russian]. Nauka, Moscow, pp. 154–157.
- Kosareva, L.R., 2018. Material Composition of Lake Bolshoe Yarovoe (Southwest Siberia) Holocene Sediments and the Sedimentary Conditions in the Area. Dr. Sci. Thesis [in Russian]. Kazansk. Gos. Univ., Kazan.
- Kosareva, L.R., Utemov, E.V., Nourgaliev, D.K., Shcherbakov, V.P., Kosarev, V.E., Yasonov, P.G., 2015. Separation of ferromagnetic components by analyzing the hysteresis loops of remanent magnetization. *Izv. Phys. Solid Earth* 51 (5), 689–708.
- Krivonogov, S.K., Gusev, V.A., Zhilich, S.V., Parkhomchuk, E.V., 2018. Intermediate lakes of the Chulym and Kargat river valleys and their role in the evolution of the Lake Chany basin. *Russian Geology and Geophysics (Geologiya i Geofizika)* 59 (5), 541–555 (673–689).
- Krylov, P.S., Nourgaliev, D.K., Yasonov, P.G., 2015. The manifestation of gas in Lake Bolshoe Yarovoe sediments according to the seismic data. *Uch. Zap. Kazansk. Univ., Ser. Estestvenn. Nauki*, 157 (4), 73–81.
- Lee, D., Seung, H., 2001. Algorithms for non-negative matrix factorization, in: *Advances in Neural Information Processing Systems 13: Proc. of the 2000 Conf.* MIT Press, Cambridge, pp. 556–562.
- Mackereth, F.J.H., 1958. A portable core sampler for lake deposits. *Limnol. Oceanogr.* 3 (2), 181–191.
- Nourgaliev, D.K., Yasonov, P.G., 2009. Coercive Spectrometer. The Patent of the Russian Federation for Utility Model no. 81805. Bull. FIPS, March 27.
- Nourgaliev, D.K., Borisov, A.S., Heller, F., Bourov, B.V., Jasonov, P.G., Khasanov, D.I., Ibragimov, Sh.Z., Heller, F., 1996. Geomagnetic secular variation through the last 3500 years as recorded by Lake Aslikul sediments from eastern Europe (Russia). *Geophys. Res. Lett.* 23 (4), 375–378.
- Obrochta, S.P., Miyahara, H., Yokoyama, Y., Crowley, T.J., 2012. A re-examination of evidence for the North Atlantic “1500-year cycle” at Site 609. *Quat. Sci. Rev.* 55, 23–33.
- Prentice, I.C., Guiot, J., Huntley, B., Jolly, D., Cheddadi, R., 1996. Reconstructing biomes from palaeoecological data: a general method and its application to European pollen data at 0 and 6 ka. *Clim. Dyn.* 12 (3), 185–194.
- Rudaya, N.A., Nazarova, L., Nourgaliev, D.K., Palagushkina, O.V., Papin, D., Frolova, L., 2012. Mid-late Holocene environmental history of Kulunda, southern West Siberia: Vegetation, climate and humans. *Quat. Sci. Rev.* 48, 32–42.
- Sholpo, L.E., 1977. *The Application of Rock Magnetism to Geological Problems* [in Russian]. Nedra, Leningrad.
- Sidorenko, M.N., 1972. *Geography of the Altai Territory* [in Russian]. Altaisk. Knizhn. Izd., Barnaul.
- Solotchina, E.P., Bezrukova, E.V., Solotchin, P.A., Shtok, O., Zhdanova, A.N., 2018. Late Pleistocene-Holocene sedimentation in lakes of central Transbaikalia: implications for climate and environment changes. *Russian Geology and Geophysics (Geologiya i Geofizika)* 59 (11), 1419–1432 (1777–1794).
- Sun, Q.L., Wang, S.M., Zhou, J., Chen, Z., Shen, J., Xie, X., Wu, F., Chen, P., 2010. Sediment geochemistry of Lake Daihai, north-central China, implications for catchment weathering and climate change during the Holocene. *J. Paleolimnol.* 43 (1), 75–87.
- Tarasov, P.E., Webb III, T., Andreev, A.A., Afanas'eva, N.B., Berezhina, N.A., Bezusko, L.G., Blyakharchuk, T.A., Bolikhovskaya, N.S., Cheddadi, R., Chernavskaya, M.M., Chernova, G.M., Dorofeyuk, N.I., Dirksen, V.G., Elina, G.A., Filimonova, L.V., Glebov, F.Z., Guiot, J., Gunova, V.S., Harrison, S.P., Jolly, D., Khomutova, V.I., Kvavadze, E.V., Osipova, I.M., Panova, N.K., Prentice, I.C., Saarse, L., Sevastyanov, D.V., Volkova, V.S., Zernitskaja, V.P., 1998. Present-day and mid-Holocene biomes reconstructed from pollen and plant macrofossil data from the former Soviet Union and Mongolia. *J. Biogeogr.* 25 (6), 1029–1053.
- Wang, W., Feng, Z.D., Ran, M., Zhang, C.J., 2013. Holocene climate and vegetation changes inferred from pollen records of Lake Aibi, northern Xinjiang, China: A potential contribution to understanding of Holocene climate pattern in East-central Asia. *Quat. Int.* 311, 54–62.
- Zhilich, S., Rudaya, N., Krivonogov, S., Pozdnyakov, D., Nazarova, L.B., 2017. Environmental dynamics of the Baraba forest-steppe (Siberia) over the last 8000 years and their impact on the types of economic life of the population. *Quat. Sci. Rev.* 163, 152–161.
- Zhong, W., Pen, Z., Xue, J., Ouyang, J., Tang, X., Cao, J., 2012. Geochemistry of sediments from Barkol Lake in the westerly influenced northeast Xinjiang: Implications for catchment weathering intensity during the Holocene. *J. Asian Earth Sci.* 50, 7–13.
- Zhou, J., Wang, S., Yang, G., Xiao, H., 2007. Younger Dryas Event and Cold Events in Early-Mid Holocene: Record from the sediment of Erhai Lake. *Adv. Clim. Change Res.*, 3 (Suppl.), 1673–1719.